Structural determinants of the dopamine transporter regulation mediated by G proteins

Genoveva Rojas[1,‡], Ivana Orellana[1,‡], Roberto Rosales-Rojas[1], Jennie García-Olivares[2], Jeffrey Comer[3], Ariela Vergara-Jaque[1,4,*]

[1]Center for Bioinformatics and Molecular Simulation, Universidad de Talca, 2 Norte 685, Talca, Chile.

[2]Supernus Pharmaceuticals. 9715 Key West Ave, Rockville MD 20850, USA.

[3]Institute of Computational Comparative Medicine, Nanotechnology Innovation Center of Kansas State, Kansas State University, Manhattan, KS 66506, USA.

[4]Millennium Nucleus of Ion Channels-associated Diseases (MiNICAD), Chile.

[‡] These authors contributed equally to this work.

* To whom correspondence should be addressed: E-mail: arvergara@utalca.cl. Telephone: +56-71-2203041.

Keywords: DAT, Gβγ subunits, neurotransmitter transporters, dopamine, protein-protein interactions, molecular dynamics simulation.

Abbreviations: DAT, dopamine transporter; Gβγ, G-protein βγ subunits; TCDB, transporter classification database; NSS, neurotransmitter:sodium symporter; MD, molecular dynamics.

ABSTRACT

Dopamine clearance in the brain is controlled by the dopamine transporter (DAT), a protein residing in the plasma membrane, which drives reuptake of extracellular dopamine into presynaptic neurons. Studies have revealed that the βγ subunits of heterotrimeric G proteins modulate DAT function through a physical association with the C-terminal region of the transporter. Regulation of neurotransmitter transporters by Gβγ subunits is unprecedented in the literature, therefore, it is interesting to investigate the structural details of this particular protein-protein interaction. Here, we refined the crystal structure of the *Drosophila melanogaster* DAT (dDAT), modeling *de novo* the N- and C-terminal domains; subsequently, we used the full-length dDAT structure to generate a comparative model of human DAT (hDAT). Both proteins were assembled with Gβ1γ2 subunits employing protein–protein docking, and subsequent molecular dynamics simulations were run to identify the specific interactions governing the formation of the hDAT:Gβγ and dDAT:Gβγ complexes. A [L/F]R[Q/E]R sequence motif containing the residues R588 in hDAT and R587 in dDAT was found as key to bind the Gβγ subunits through electrostatic interactions with a cluster of negatively charged residues located at the top face of the Gβ subunit. Alterations of DAT function have been associated with multiple devastating neuropathological conditions; therefore, this work represents a step toward better understanding DAT regulation by signaling proteins, allowing us to predict therapeutic target regions.

INTRODUCTION

The sodium-dependent dopamine transporter (DAT) is a plasma membrane protein that regulates dopamine homeostasis within the brain by driving the energetically "uphill" movement of extracellular dopamine into presynaptic neurons, which is coupled to pre-existing sodium and chloride transmembrane gradients[1]. Dopamine translocation occurs by an alternating-access mechanism[2], in which DAT cycles between outwardly and inwardly facing conformations that bind and release dopamine on opposite sides of the membrane. DAT is encoded by the SLC6A3 gene, located on the human chromosome 5q15.3[3], and belongs to the neurotransmitter:sodium

symporter (NSS) family (TCDB: 2.A.22)[4]. As revealed in the *Drosophila melanogaster* DAT (dDAT) crystal structure[5,6], this protein exhibits an overall LeuT-like fold with 12 transmembrane segments symmetrically organized in two inverted repeating units (transmembrane helices (TMs) 1–5 and TMs 6–10) with the N- and C-terminal domains exposed to the cytoplasm.

Members of the NSS family are recognized by their critical role in regulating neurotransmission and are targets for psychostimulants, anti-depressants and other drugs. In fact, dysfunction of DAT has been associated with multiple neurological and psychiatric disorders, such as bipolar and attention deficit/hyperactivity disorder, schizophrenia, Parkinson's disease, Tourette's syndrome, Angelman's syndrome, and drug addiction[7,8]. Several psychotherapeutic agents and drugs of abuse (e.g., cocaine and amphetamines) bind to DAT, either enhancing or inhibiting its function[9]. Moreover, DAT function has shown to be regulated by a plethora of intracellular and extracellular mechanisms including protein–protein interactions. Numerous efforts have led to the identification of proteins that interact with DAT and modulate either its catalytic activity or trafficking. These proteins include Syntaxin 1A (Syn1A), D_2 DA receptors, calcium-calmodulin dependent protein kinase (CaMK), α-synuclein and other scaffolding proteins[10].

A functional interaction has been identified between human DAT (hDAT) and heterotrimeric G proteins. Co-immunoprecipitation assays revealed a physical association between the transporter and βγ subunits of G-protein, whereas Immuno-Far Western blotting demonstrated a direct interaction of these subunits with the carboxy-terminal domain of hDAT[11]. Activation of G proteins occurs when guanosine triphosphate (GTP) binds to the α subunit of the Gαβγ trimeric complex, resulting in the separation of the βγ subunits[12]. Overexpression or activation of endogenous Gβ1γ2 proteins (the most common Gβγ isoforms expressed in brain) in presence of hDAT exhibited a reduction of the dopamine uptake, demonstrating an inhibitory effect on DAT activity. Moreover, Gβγ subunits showed to induce outward dopamine transport through DAT, in a process referred to as "efflux"[13]. Key residues involved in this particular protein–protein interaction were also identified by evaluating peptide fragments of the DAT

carboxy terminus to bind Gβγ subunits. Residues 582 to 596 in the hDAT were found as the primary binding site of G proteins.

Taken together, these lines of evidence establish important aspects on DAT regulation by protein–protein interactions, which has emerged as a promising pharmacological target. Gβγ subunits were previously reported to directly modulate several effector macromolecules including ion channels, enzymes, and intracellular regulators[14,15]; however, DAT is the first neurotransmitter transporter found to be regulated by G proteins. Motivated by these findings, here we used bioinformatics and computational structural biology approaches to reveal the structural basis of the protein–protein interaction between human and *Drosophila melanogaster* DAT and Gβγ subunits. Specifically, we modeled the missing N- and C-terminal domains *de novo* onto the dDAT crystal structure and built a homology model of hDAT. The full-length structures of both transporters were then used to generate molecular assemblies with Gβγ subunits and to describe the specific interactions at the binding interface of each complex. This work is expected to be crucial for structure-based drug design as well as for identifying key residues linked to regulation of the dopamine transporter by external proteins.

METHODS

Modeling of the N- and C-terminal domains of dDAT. An X-ray structure of DAT from *Drosophila melanogaster* (dDAT) bound to L-dopamine was recently elucidated (PDB ID 4XP1)[6]. This crystal structure includes residues 25 to 600; therefore, the folded structure of the first 24 amino acids of the N-terminal domain and last 31 amino acids of the C-terminal domain (residues 601 to 631) remain unknown. To model the missing residues in the dDAT structure, secondary structure prediction and fragment-based *de novo* modeling were carried out. Secondary structure propensities for the full-length dDAT sequence were estimated using the servers PsiPred v4.0[16] and PSSpred[17]. In addition, protein compactness and local secondary structural features were estimated with the "protein meta-structure" approach implemented by Konrat R[18]. Structural models of the N- and C-terminal domain of dDAT were generated through the standard ROSETTA *ab initio* protocol[19,20]. In preparation for modeling, 3-mer and 9-mer fragment library files were

created with the ROBETTA server[21], identifying protein-fragment structures in the Protein Data Bank that are compatible with the dDAT sequence. Based on these libraries, 20,000 dDAT models were built including the missing N- and C-terminal residues and keeping fixed the known structure of the protein during the conformational searching. To identify distinct folds of the termini, the models were clustered with the ROSETTA cluster application using a root-mean-square deviation (RMSD) cutoff value of 7 Å. The structures with the lowest ROSETTA score in each cluster were chosen as representative (Figure S1) and analyzed with the PROCHECK[22] and ProQM[23] scoring functions. The best model was selected as that with the highest score in the most populated cluster. The final model is of excellent quality according to PROCHECK, with 99.2% of the residues in the favored and additional allowed regions of the Ramachandran plot. The global ProQM score reached a value of 0.686, where 0.7 is typical for membrane protein structures solved by X-ray crystallography. To improve the local backbone orientation and to minimize side-chain steric clashes, the final model was relaxed using the ROSETTA relax application.

Homology modeling of hDAT. To model hDAT, the full-length dDAT refined structure was used as a template. The pairwise sequence alignment between dDAT and hDAT was generated using the AlignMe server v1.1 in PS mode[24]. A total of 2,000 hDAT models were built using MODELLER v9.18[25]. The best model was selected as that with the lowest Molpdf energy value of MODELLER and the highest PROCHECK[22] and global ProQM[23] scores. Due to the differences in size of the N- and C-terminal domains of hDAT as compared to dDAT, after model the entire hDAT structure a refinement only of the termini was performed with ROSETTA *ab initio*[19,20]. The same protocol described previously for modeling the N- and C-terminal domains in dDAT was used, generating 10,000 hDAT conformations and selecting the best model as that with the highest scores. The final hDAT model agrees with PsiPred v4.0[26] secondary structure and TOPCONS v2.0[27] transmembrane predictions. dDAT and hDAT were structurally compared using PyMOL v1.8.4 (Schrödinger, LLC). The position of hDAT in the membrane was defined by its superposition onto dDAT, which was determined with the Orientation of Proteins in Membranes (OPM) server[28].

Protein–protein docking between dDAT/hDAT and Gβγ subunits. The full-length dDAT and hDAT models were used to generate molecular assemblies with G-protein βγ subunits. The crystal structure of Gβ1γ2 (PDB ID 1XHM)[29], bound to a small SIGK peptide that facilitates the Gα dissociation, was used for performing molecular docking calculations. The SIGK peptide was removed to permit dDAT/hDAT interaction with Gβγ. Based on previous experimental data for human DAT[11], the C-terminal region of dDAT and hDAT was selected as the contact area to accommodate free motion of the Gβγ subunits. In the same way, the surface of the Gβ subunit interacting with the SIGK peptide was defined to interact with the transporters. A first docking approach was performed with HADDOCK v2.2[30], generating 1,000 docking conformations in each case. The best dDAT:Gβγ and hDAT:Gβγ complexes were selected according to the HADDOCK scoring function. Subsequently, to perform a more exhaustive search of the conformational space of the Gβγ subunits, additional 50,000 docking conformations for each complex were generated with the Monte Carlo based multi-scale docking algorithm implemented in ROSETTA[31]. Analyses of the ROSETTA docking interface score against the C_α RMSD of each conformation relative to the starting docking complex (the lowest-scoring HADDOCK model) were used to evaluate docking convergence, and to select the final hDAT:Gβγ and dDAT:Gβγ complexes. The binding mode of the hDAT and dDAT with the Gβ subunit, with special emphasis at the C-terminal region of the transporters, was compared with that of the SIGK peptide in the Gβγ crystal structure using PyMOL v1.8.4 (Schrödinger, LLC). Electrostatic surface potential analyses were performed with the PyMOL APBS Tools v2.1[32].

Molecular dynamics simulation of the dDAT/hDAT:Gβγ complexes. The lowest scoring conformation of each complex obtained from docking – namely, dDAT:Gβγ and hDAT:Gβγ – was used as a starting point to perform molecular dynamics (MD) simulations. Each complex was embedded in a fully hydrated palmitoyl-oleyl-phosphatidyl-choline (POPC) bilayer solvated with explicit water molecules. A dopamine molecule adjacent to two sodium ions and one chloride ion were included in each complex as revealed in the dDAT crystal structure[6]. The dopamine parameters were obtained from the ParamChem server, using the CGenFF force field.[33] Sodium and chloride ions (0.15 M NaCl) were added to the aqueous phase to mimic physiological

conditions and to ensure charge neutrality. The protonation states of the titratable residues in the proteins were checked at neutral pH using the PropKa program[34]. The initial configuration of the systems was optimized by means of a 30,000-step energy minimization, followed by equilibration and relaxation in a 108 ns MD simulation in the isobaric-isothermal ensemble. Soft harmonic restraints were applied to the proteins and substrates during the first 8 ns of simulation, which were gradually decreased from 20 to 0 kcal mol^{-1} $Å^{-2}$. The distance between dDAT/hDAT and the Gβγ subunits was also restrained using the collective variable module (Colvars)[35]. At the end of the 108 ns of simulation for each system, three equilibrated conformations were selected and simulated for additional 100 ns without restraints, totaling 408 ns in each case (three replicas). The masses of hydrogen atoms for the proteins and lipids were increased by a factor of 3 by transferring the mass of heavy atoms into the bonded hydrogen atoms[36]; accordingly, the time step for all MD simulations was 4 fs. The temperature (300 K) was maintained using a Langevin thermostat with a damping coefficient of 1 ps^{-1}. The pressure (1 atm) was controlled by the Langevin piston method[37]. Long-range electrostatic interactions were computed using the particle-mesh Ewald summation method[38], with a smooth real-space cutoff applied between 8 and 9 Å. All covalent bonds involving hydrogen as well as the intramolecular geometries of water were constrained using the SETTLE algorithm[39]. All MD simulations were performed using the program NAMD v2.12[40] and the CHARMM[41] force field. The root mean-square deviation (RMSD) of the residues at the binding interface of the protein complexes were utilized to assess stability and thermodynamic equilibrium (Figure S2). Structural analyses of the systems were performed using VMD v1.9.3 software[42]. Distances between the side chains of residues located in the binding region of dDAT/hDAT and the Gβ subunit were evaluated during the simulations. Contact maps were generated by averaging these distances over the three replica simulations.

Sequence analysis of DAT homologs. Protein sequences of known members of the neurotransmitter:sodium symporter family (NSS, transporter classification database [TCDB] 2.A.22) were obtained from the UniprotKB database[43]. Five protein sequences were compared – namely, the dopamine transporter (DAT) and serotonin transporter (SERT) from *Homo sapiens*

and *Drosophila melanogaster*, and the *Homo sapiens* norepinephrine transporter (NET). A multiple-sequence alignment was built with MAFFT v7.31[44] and analyzed with Jalview v2.10.1[45].

RESULTS

Modeling of structurally unresolved residues in the dDAT structure. Based on previous reports describing the importance of cytoplasmic terminal segments in membrane transporters in acting as primary targets of protein–protein interactions[11,46,47], we modeled the missing N- and C-terminal domains in the dDAT structure bound to L-dopamine (PDB ID 4XP1)[6]. Our main challenge was modeling the association of the full-length dDAT structure with Gβγ subunits, which has been demonstrated in experiments[11,13]. The missing fragments in the dDAT structure comprise residues 1 to 24 at the N-terminus and residues 601 to 631 at the C-terminus (Figure 1A). The most prevalent secondary structure in both regions was estimated through the secondary structure prediction algorithms implemented in PsiPred[16] and PSSpred[17]. For the N-terminal domain, no secondary structural elements were identified, whereas small α-helical portions were predicted in the C-terminal region (Figure 1B). This latter region is of particular interest in our study because it has been recognized as the anchoring region of Gβγ subunits[11,13]; therefore, additional predictions of local compactness and secondary structure were applied using the so-called protein meta-structure approach[18]. Large residue-specific compactness values are assigned to residues that are buried deep in the interior of a protein structure. As shown in Figure 1C, the overall compactness of the dDAT C-terminal domain is expected to be high. In addition, secondary structure predictions from the meta-structure method[18] (Figure 1D) confirm that helical elements appear mostly along residues 600 to 606 (Figure 1D), which is represented by positive values in the secondary structure *vs.* residue positions plot.

The full-length dDAT structure modeled with the ROSETTA *ab initio* protocol[19,20] is shown in Figure 1E. Ten different folds of the termini were identified by clustering the first 1,000 lowest scoring models at a RMSD of 7 Å (Figure S1). We selected as representative the structure with the lowest score from the cluster containing the majority of the conformers. However, we do not rule out that another model of our set may be equally probable. The N-terminal domain, although not relevant for interaction with Gβγ subunits, adopts a random coil structure in agreement with

secondary structure analyses, whereas the C-terminal domain is formed of small α-helical fragments, which appear to establish intramolecular contacts with the rest of the protein. Our model provides the first structure-based insights into the tertiary arrangement of the N- and C-terminal domains in the dopamine transporter considering spatial restraints of surrounding residues from the transmembrane region. Structures previously reported[48,49] correspond to models of N- and C-terminal fragments in free solution, which certainly not represent the conformation adopted onto the full-length protein.

Structural model of hDAT based on dDAT. Several comparative models of hDAT have been previously built[50–52] to explore questions related to the transporting process and mechanisms for substrate selectivity of this transporter. In the present study, in order to ensure consistency in the comparisons of sequence and structural similarity between hDAT and dDAT, we built a homology model of hDAT from our full-length refined dDAT model using our standard modeling protocol for membrane proteins[53,54]. dDAT has 49.36% sequence identity with hDAT, as estimated over the whole sequences, and reaches a similarity of ≈64% (Figure 2A). The region comprising the transmembrane segments of both proteins is highly conserved; however, hDAT exhibits some differences at the N- and C-termini, and in the loop between the S3 and S4 segments. The overall core of hDAT was modeled based on the refined dDAT structure using MODELLER[25], whereas the N-terminal and C-terminal domains were refined by *ab initio* modeling with ROSETTA[19,20]. The final hDAT model (Figure 2B) contains a longer N-terminal domain and a shorter C-terminal domain as compared to dDAT.

Garcia-Olivares et al.[13] demonstrated that residues 582 to 596 situated at the hDAT C-terminus (581–595 in dDAT) play an important role in the interaction with Gβγ subunits; therefore, reproducing the complete structure of the C-terminal domain might be relevant to describe the association of hDAT with G proteins. Moreover, based on the sequence identity and secondary structure predictions, here we hypothesize that dDAT is also regulated by Gβγ subunits. The hDAT C-terminal domain shows similar structural elements to those found in dDAT (Figure 2C) – namely, small α-helical fragments and compactness of the residues exposed to the

intracellular medium, which makes us to suggest a conserved structural mechanism to bind βγ subunits of G proteins.

Molecular assembly of hDAT/dDAT with Gβγ subunits. The hDAT and dDAT models with the N-terminal and C-terminal domains built *de novo* were used to generate a molecular assembly of each transporter with the G-protein βγ subunits using HADDOCK[30] and the ROSETTA protein–protein docking protocol[31]. Heterotrimeric G proteins are composed of α, β, and γ subunits; however, after a signaling cascade, the βγ subunits are separated from the α subunit and exist as a constitutive functional dimer. Of the two subunits, only the Gβ subunit makes contact with the C-terminal domains of hDAT and dDAT in the lowest scoring protein–protein assemblies obtained by docking (Figure 3A-B). The Gγ subunit in both cases is coupled to the Gβ subunit facing the intracellular medium. Because dDAT has a longer C-terminal region than hDAT, dDAT exposes a bigger contact surface for binding the Gβ subunit (Figure 3B). It should be noted that the validity of docked structures obtained from ROSETTA[31] can be judged by verifying the presence of an energetic binding funnel, obtained by plotting the interface score of the docking conformers as a function of the Cα RMSD relative to the starting conformation. Protein–protein docking evaluating the formation of the hDAT:Gβγ and dDAT:Gβγ complexes showed clear energetic binding funnels, which indicates convergence of the calculations.

As shown in Figure 3C, the region of the Gβ subunit interacting with hDAT and dDAT is the same region where the SIGK peptide is bound in the crystal structure of the Gβγ dimer[29]. Interestingly, this region has been shown to be important for recognition of most Gβγ-associated targets[15,55,56]. The lysine residue at position 4 of the SIGK peptide participates as an anchoring point to bind the Gβ subunit (Figure 3D). An electrostatic potential surface analysis projected over this subunit showed a negatively charged region serving as the binding site for K4. In the same way, through a visual inspection of the docked poses of the hDAT/dDAT:Gβγ complexes, we found that residues R588 in hDAT and R587 in dDAT make contact with the Gβ subunit in an orientation equivalent to that exhibited by K4 of the SIGK peptide. These arginine residues establish electrostatic interactions with a cluster of negatively charged amino acids comprising three aspartic acids at positions 186, 228 and 246 of the Gβ subunit.

Molecular determinants for the binding of hDAT/dDAT to Gβγ subunits. To identify key interactions in the binding interface of the two complexes modeled by docking (i.e. hDAT:Gβγ and dDAT:Gβγ), we ran MD simulations applying the CHARMM[41] force field and mimicking the physiological environment of the proteins as shown in Figure 4A. Average distances between the centers of mass of the residue's side chains of hDAT and dDAT and the G-protein β subunit were calculated during the equilibrated MD trajectories (Figure 4B-C) in order to determine the most prevalent interactions. Three independent replica simulations were run for each complex, which exhibited equivalent interfacial interactions between the proteins, indicating reproducibility of the data (Figure S3). For the hDAT:Gβγ complex, residues along the positions 585 and 595 of the transporter showed close contacts (distances of ≈5 Å) with residues between positions 140 to 250 of the Gβ subunit. This contact region of hDAT is of particular interest because *in vitro* binding assays demonstrated that the Gβγ subunits bind directly to the fragment corresponding to S582 through A596[13]; therefore, the predicted interatomic distances in the modeled complex are consistent with existing experimental data. Moreover, alanine substitutions of residues 587 to 590 (sequence FREK) abolished the binding of Gβγ subunits, which agrees with a structural analysis of the C-terminal region of hDAT binding the Gβγ subunits, where residues F587, R588, E589 and K590 of hDAT interact with residues W99, Y145, D186, D228, D246 and N230 of Gβ (Figure 4D). Additional contacts are observed around residues 605 to 610 of hDAT (Figure S4), however, experimental data not demonstrated a significant contribution of this region to bind Gβγ subunits. In the case of dDAT:Gβγ, even though the contour map of the average distances shows a greater number of contacts between the proteins, we focused on the region comprising residues 580 to 590 to evaluate whether dDAT makes contacts similar to those made by hDAT. As shown in Figure 4E, residues L586, R587, Q588 and R589 of dDAT were closest to the Gβ subunit, interacting with residues K57, Y59, M188, D186, D228, N230, D246 and W322. As was previously revealed by docking calculations, the interactions of R588 in hDAT and R587 in dDAT with the residues D186, D228, and D246 were fairly preserved throughout the MD simulations (Figure S5), demonstrating the importance of these residues. It should be noted that protonated states of the aspartic residues could be found due to the electrostatic environment at the binding

interface of the complexes; however, we only analyzed the unprotonated states of these residues.

Residues predicted to bind Gβγ subunits in NSS family members. The conservation of key residues for binding hDAT and dDAT with Gβγ subunits was evaluated against five members of the neurotransmitter:sodium symporter family (Figure 4F). Interestingly, we identified conservation of the FREK and LRQR sequences of hDAT and dDAT, respectively, in the serotonin transporter (SERT) from human and *Drosophila melanogaster*, and the human norepinephrine transporter (NET). In particular, the arginine residues anchoring the Gβ subunit in hDAT and dDAT are equivalent to R597 of *Drosophila melanogaster* SERT and K605 from human SERT. We hypothesize, therefore, that a [L/F]R[Q/E]R motif is required to bind G-protein βγ subunits to neurotransmitter transporters.

DISCUSSION

Penmatsa et al. in 2013 reported the first crystal structure of the dopamine transporter from *Drosophila melanogaster* (dDAT) in an inactive state[5]. Subsequently, in 2015 the same authors revealed new dDAT structures in a transport-active conformation bound to different substrates: the natural DAT substrate dopamine, the substrate analogue 3,4-dichlorophenethylamine, the psychostimulants D-amphetamine and methamphetamine, and cocaine analogues[6]. None of these structures, however, represent a full-length sequence protein, limiting our understanding of the role played by certain residues for the functioning of DAT; particularly, those residues constituting the N- and C-terminal domains. Previous reports have revealed the importance of cytoplasmic terminal segments in participating as primary targets in the formation of protein–protein interactions in membrane transporters . Large N- and C-terminal segments in the cytoplasmic region have been shown to contain sites for post-translational modifications, regulatory motifs, and interacting with binding partners[7]. In the case of DAT, Garcia-Olivares et al. in 2013 identified a functional interaction of the transporter with heterotrimeric G-proteins through a physical association of the Gβγ subunits with the C-terminal domain of human DAT. Based on that evidence, we modeled the missing residues at the N- and C-terminal domains of

the dDAT crystal structure by *de novo,* and subsequently generated a homology model of hDAT using the full-length dDAT structure as a template. We used dDAT in our study because is the closest hDAT homologue with crystal structure available and it has become a recognized target to study pharmacology and substrate specificity in different neurotransmitter sodium symporters. *De novo* and homology-based modeling, despite their limited resolution, allow prediction of coarse structural features of proteins, which can help to explain existing experimental data, and also help to describe regulatory and functional mechanisms in a structural context[58]. Here we present full-length models of dDAT and hDAT structures based on a consistent and robust *de novo* and homology modeling protocol, which represent a significant advance in comparing both structures and in analyzing their association with effector molecules and other proteins regulating their function.

DAT and other members of the NSS family have long N- and C-terminal domains that share certain similarities, consistent with the possible role of these regions in modulating specific regulation of neurotransmitter transporters through intracellular protein–protein interactions and post-translational modifications. Binding of G-protein βγ subunits to the C-terminal domain of human DAT has been demonstrated to regulate its activity, particularly, inducing a dopamine efflux[11,13]. Alterations on dopamine transporter may have important implications in the homeostasis of this neurotransmitter generating severe neurological disorders. In this regard, the binding interface of human DAT with Gβγ subunits has become an important pharmacological target. Human DAT shares ≈50% sequence identity with *Drosophila melanogaster* DAT and both proteins are close homologues of noradrenaline transporters (NETs) and serotonin transporters (SERTs); hence, study of the pharmacology, substrate specificity, and protein–protein interactions of DAT in different organisms (human and invertebrate) may aid to the general understanding of the members of the NSS family. In the present study, we hypothesize that dDAT, like hDAT, is regulated by Gβγ subunits. Accordingly, we used computational methods to predict the molecular assembly of both transporters with G-proteins. The proposed models correspond to the lowest-energy conformation of the complexes obtained by protein-protein docking and MD simulations, which are likely representative states of one of many possible interaction modes between the proteins. Gβγ subunits were predicted to bind to the C-terminal segments of both

hDAT and dDAT, interacting with a structural domain shared by the two transporters, namely, the FREK and LRQR sequences, respectively. We found these positively charged domains bound to the same pocket of negatively charged residues in the Gβ subunit. Interestingly, this pocket has been found at the binding interface of others Gβγ-associated targets, including GIRK channels[15], protein kinases[55], nanobodies[56], and G protein-coupled receptors[59]. Moreover, as previously mentioned, this pocket constitutes the binding site of the SIGK peptide in the Gβγ dimeric crystal structure[29].

The X-ray structure of the SIGK peptide bound to the Gβγ subunits[29] shows that a cluster of aspartic acid residues (D186, D228 and D246) located at the top face of Gβ subunit make contact with the positively charged residue K4 of the peptide. Similarly, our analyses predict that this same cluster of aspartic acid residues interact strongly with homologous positive regions of hDAT and dDAT, having sequences of FREK and LRQR, respectively. In previous experiments[10], alanine substitution of the FREK sequence in hDAT (only residues 587–590) was sufficient to abolish DAT down-regulation by protein kinase C. Similar residues have been proposed to bind the coat protein complex II (COPII) component, Sec24D, in several NSS proteins suggesting a key role of this region in regulating DAT and other neurotransmitter transporters[10]. Our study, therefore, supports the importance of a conserved positively charged motif at the C-terminal domain of human and *Drosophila melanogaster* DAT acting as an anchoring point to bind Gβγ subunits. Notably, residue R101 in the CDR3 loop of a llama-derived nanobody was identified as key for binding G-protein β subunits[56], whereas K663 in the C-terminal loop of G protein-coupled receptor kinase 2 (GRK2) was also found essential for the formation of the GRK2-Gβ1γ2 complex[55]. These analyses indicate a similar mode of interaction among proteins that bind G-protein βγ subunits. In fact, our analysis of the conservation of residue R588 in hDAT (R587 in dDAT) among members of the NSS family revealed homologous residues in the C-terminal domains of the serotonin and norepinephrine transporters, allowing us to hypothesize that these residues are also key contributors to binding of G-proteins, extending the significance of our study beyond the dopamine transporter.

CONCLUSIONS

Substantial evidence supports that pharmaceuticals and drugs of abuse modifying dopamine signaling, as well as G-protein βγ subunits, alter multiple DAT regulatory processes, affecting substrate tracking and stimulating the efflux of dopamine. The present work represents an extensive structural characterization for understanding the molecular determinants of DAT regulation mediated by Gβγ subunits. Specifically, we generated a molecular model of the hDAT:Gβγ complex and validated it against existing experimental data. Moreover, we identified previously unknown intermolecular interactions between the Gβγ subunits and the *Drosophila melanogaster* DAT. The predicted structural assemblies of both complexes certainly will require experimental confirmation. However, an improved understanding of the molecular basis of binding between dopamine transporters and Gβγ subunits in different organisms should lead to the study of associated mutations and the identification of target regions for pharmaceutical compounds that modulate the function of DAT and other neurotransmitters.

AUTHOR CONTRIBUTIONS

A.V-J and J.G-O conceived the project. A.V-J and J.C participated in designing the computational studies. G.R, I.O, and R.R-R carried out computational modeling and simulations. A.V-J supervised computational simulations efforts and wrote the manuscript. All authors contributed to the editing of the paper and to scientific discussions.

ACKNOWLEDGMENT

A.V-J. thanks FONDECYT research initiation grant #11170223. The Millennium Nucleus of Ion Channels-Associated Diseases (MiNICAD) is a Millennium Nucleus supported by the Iniciativa Científica Milenio of the Ministry of Economy, Development and Tourism (Chile). We acknowledge partial support from US National Science Foundation grant CHE-1726332.

REFERENCES

(1) Ciliax, B. J.; Heilman, C.; Demchyshyn, L. L.; Pristupa, Z. B.; Ince, E.; Hersch, S. M.; Niznik, H. B.; Levey, A. I. The Dopamine Transporter: Immunochemical Characterization and Localization in Brain. *J. Neurosci. Off. J. Soc. Neurosci.* **1995**, *15* (3 Pt 1), 1714–1723.

(2) Forrest, L. R.; Zhang, Y.-W.; Jacobs, M. T.; Gesmonde, J.; Xie, L.; Honig, B. H.; Rudnick, G. Mechanism for Alternating Access in Neurotransmitter Transporters. *Proc. Natl. Acad. Sci. U. S. A.* **2008**, *105* (30), 10338–10343. https://doi.org/10.1073/pnas.0804659105.

(3) Vandenbergh, D. J.; Persico, A. M.; Hawkins, A. L.; Griffin, C. A.; Li, X.; Jabs, E. W.; Uhl, G. R. Human Dopamine Transporter Gene (DAT1) Maps to Chromosome 5p15.3 and Displays a VNTR. *Genomics* **1992**, *14* (4), 1104–1106. https://doi.org/10.1016/s0888-7543(05)80138-7.

(4) Rudnick, G.; Krämer, R.; Blakely, R. D.; Murphy, D. L.; Verrey, F. The SLC6 Transporters: Perspectives on Structure, Functions, Regulation, and Models for Transporter Dysfunction. *Pflugers Arch.* **2014**, *466* (1), 25–42. https://doi.org/10.1007/s00424-013-1410-1.

(5) Penmatsa, A.; Wang, K. H.; Gouaux, E. X-Ray Structure of Dopamine Transporter Elucidates Antidepressant Mechanism. *Nature* **2013**, *503* (7474), 85–90. https://doi.org/10.1038/nature12533.

(6) Wang, K. H.; Penmatsa, A.; Gouaux, E. Neurotransmitter and Psychostimulant Recognition by the Dopamine Transporter. *Nature* **2015**, *521* (7552), 322–327. https://doi.org/10.1038/nature14431.

(7) Vaughan, R. A.; Foster, J. D. Mechanisms of Dopamine Transporter Regulation in Normal and Disease States. *Trends Pharmacol. Sci.* **2013**, *34* (9), 489–496. https://doi.org/10.1016/j.tips.2013.07.005.

(8) Blakely, R. D. Dopamine Transporters: Chemistry, Biology, and Pharmacology. *Q. Rev. Biol.* **2010**, *85* (1), 103–104. https://doi.org/10.1086/650250.

(9) Zhu, J.; Reith, M. E. A. Role of the Dopamine Transporter in the Action of Psychostimulants, Nicotine, and Other Drugs of Abuse. *CNS Neurol. Disord. Drug Targets* **2008**, *7* (5), 393–409.

(10) Eriksen, J.; Jørgensen, T. N.; Gether, U. Regulation of Dopamine Transporter Function by Protein-Protein Interactions: New Discoveries and Methodological Challenges. *J. Neurochem.* **2010**, *113* (1), 27–41. https://doi.org/10.1111/j.1471-4159.2010.06599.x.

(11) Garcia-Olivares, J.; Torres-Salazar, D.; Owens, W. A.; Baust, T.; Siderovski, D. P.; Amara, S. G.; Zhu, J.; Daws, L. C.; Torres, G. E. Inhibition of Dopamine Transporter Activity by G Protein Bγ Subunits. *PloS One* **2013**, *8* (3), e59788. https://doi.org/10.1371/journal.pone.0059788.

(12) Clapham, D. E.; Neer, E. J. G Protein Beta Gamma Subunits. *Annu. Rev. Pharmacol. Toxicol.* **1997**, *37*, 167–203. https://doi.org/10.1146/annurev.pharmtox.37.1.167.

(13) Garcia-Olivares, J.; Baust, T.; Harris, S.; Hamilton, P.; Galli, A.; Amara, S. G.; Torres, G. E. Gβγ Subunit Activation Promotes Dopamine Efflux through the Dopamine Transporter. *Mol. Psychiatry* **2017**, *22* (12), 1673–1679. https://doi.org/10.1038/mp.2017.176.

(14) Smrcka, A. V.; Lehmann, D. M.; Dessal, A. L. G Protein Bγ Subunits as Targets for Small Molecule Therapeutic Development. *Comb. Chem. High Throughput Screen.* **2008**, *11* (5), 382–395.

(15) Whorton, M. R.; MacKinnon, R. X-Ray Structure of the Mammalian GIRK2-Bγ G-Protein Complex. *Nature* **2013**, *498* (7453), 190–197. https://doi.org/10.1038/nature12241.
(16) Buchan, D. W. A.; Minneci, F.; Nugent, T. C. O.; Bryson, K.; Jones, D. T. Scalable Web Services for the PSIPRED Protein Analysis Workbench. *Nucleic Acids Res.* **2013**, *41* (Web Server issue), W349-357. https://doi.org/10.1093/nar/gkt381.
(17) Yan, R.; Xu, D.; Yang, J.; Walker, S.; Zhang, Y. A Comparative Assessment and Analysis of 20 Representative Sequence Alignment Methods for Protein Structure Prediction. *Sci. Rep.* **2013**, *3* (1), 1–9. https://doi.org/10.1038/srep02619.
(18) Konrat, R. The Protein Meta-Structure: A Novel Concept for Chemical and Molecular Biology. *Cell. Mol. Life Sci. CMLS* **2009**, *66* (22), 3625–3639. https://doi.org/10.1007/s00018-009-0117-0.
(19) Rohl, C. A.; Strauss, C. E. M.; Misura, K. M. S.; Baker, D. Protein Structure Prediction Using Rosetta. *Methods Enzymol.* **2004**, *383*, 66–93. https://doi.org/10.1016/S0076-6879(04)83004-0.
(20) Bonneau, R.; Tsai, J.; Ruczinski, I.; Chivian, D.; Rohl, C.; Strauss, C. E.; Baker, D. Rosetta in CASP4: Progress in Ab Initio Protein Structure Prediction. *Proteins* **2001**, *Suppl 5*, 119–126.
(21) Kim, D. E.; Chivian, D.; Baker, D. Protein Structure Prediction and Analysis Using the Robetta Server. *Nucleic Acids Res.* **2004**, *32* (Web Server issue), W526–W531. https://doi.org/10.1093/nar/gkh468.
(22) Laskowski, R. A.; MacArthur, M. W.; Moss, D. S.; Thornton, J. M. PROCHECK: A Program to Check the Stereochemical Quality of Protein Structures. *J. Appl. Crystallogr.* **1993**, *26* (2), 283–291. https://doi.org/10.1107/S0021889892009944.
(23) Ray, A.; Lindahl, E.; Wallner, B. Model Quality Assessment for Membrane Proteins. *Bioinformatics* **2010**, *26* (24), 3067–3074. https://doi.org/10.1093/bioinformatics/btq581.
(24) Stamm, M.; Staritzbichler, R.; Khafizov, K.; Forrest, L. R. AlignMe—a Membrane Protein Sequence Alignment Web Server. *Nucleic Acids Res.* **2014**, *42* (Web Server issue), W246–W251. https://doi.org/10.1093/nar/gku291.
(25) Eswar, N.; Webb, B.; Marti-Renom, M. A.; Madhusudhan, M. S.; Eramian, D.; Shen, M.-Y.; Pieper, U.; Sali, A. Comparative Protein Structure Modeling Using MODELLER. *Curr. Protoc. Protein Sci. Editor. Board John E Coligan Al* **2007**, *Chapter 2*, Unit 2.9. https://doi.org/10.1002/0471140864.ps0209s50.
(26) Jones, D. T. Protein Secondary Structure Prediction Based on Position-Specific Scoring Matrices. *J. Mol. Biol.* **1999**, *292* (2), 195–202. https://doi.org/10.1006/jmbi.1999.3091.
(27) Tsirigos, K. D.; Peters, C.; Shu, N.; Käll, L.; Elofsson, A. The TOPCONS Web Server for Consensus Prediction of Membrane Protein Topology and Signal Peptides. *Nucleic Acids Res.* **2015**, gkv485. https://doi.org/10.1093/nar/gkv485.
(28) Lomize, M. A.; Lomize, A. L.; Pogozheva, I. D.; Mosberg, H. I. OPM: Orientations of Proteins in Membranes Database. *Bioinforma. Oxf. Engl.* **2006**, *22* (5), 623–625. https://doi.org/10.1093/bioinformatics/btk023.
(29) Davis, T. L.; Bonacci, T. M.; Sprang, S. R.; Smrcka, A. V. Structural and Molecular Characterization of a Preferred Protein Interaction Surface on G Protein Beta Gamma Subunits. *Biochemistry* **2005**, *44* (31), 10593–10604. https://doi.org/10.1021/bi050655i.

(30) Dominguez, C.; Boelens, R.; Bonvin, A. M. J. J. HADDOCK: A Protein-Protein Docking Approach Based on Biochemical or Biophysical Information. *J. Am. Chem. Soc.* **2003**, *125* (7), 1731–1737. https://doi.org/10.1021/ja026939x.
(31) Chaudhury, S.; Berrondo, M.; Weitzner, B. D.; Muthu, P.; Bergman, H.; Gray, J. J. Benchmarking and Analysis of Protein Docking Performance in Rosetta v3.2. *PloS One* **2011**, *6* (8), e22477. https://doi.org/10.1371/journal.pone.0022477.
(32) Baker, N. A.; Sept, D.; Joseph, S.; Holst, M. J.; McCammon, J. A. Electrostatics of Nanosystems: Application to Microtubules and the Ribosome. *Proc. Natl. Acad. Sci. U. S. A.* **2001**, *98* (18), 10037–10041. https://doi.org/10.1073/pnas.181342398.
(33) Vanommeslaeghe, K.; Hatcher, E.; Acharya, C.; Kundu, S.; Zhong, S.; Shim, J.; Darian, E.; Guvench, O.; Lopes, P.; Vorobyov, I.; MacKerell, A. D. CHARMM General Force Field (CGenFF): A Force Field for Drug-like Molecules Compatible with the CHARMM All-Atom Additive Biological Force Fields. *J. Comput. Chem.* **2010**, *31* (4), 671–690. https://doi.org/10.1002/jcc.21367.
(34) Olsson, M. H. M.; Søndergaard, C. R.; Rostkowski, M.; Jensen, J. H. PROPKA3: Consistent Treatment of Internal and Surface Residues in Empirical PKa Predictions. *J. Chem. Theory Comput.* **2011**, *7* (2), 525–537. https://doi.org/10.1021/ct100578z.
(35) Fiorin, G.; Klein, M. L.; Hénin, J. Using Collective Variables to Drive Molecular Dynamics Simulations. *Mol. Phys.* **2013**, *111* (22–23), 3345–3362. https://doi.org/10.1080/00268976.2013.813594.
(36) Hopkins, C. W.; Le Grand, S.; Walker, R. C.; Roitberg, A. E. Long-Time-Step Molecular Dynamics through Hydrogen Mass Repartitioning. *J. Chem. Theory Comput.* **2015**, *11* (4), 1864–1874. https://doi.org/10.1021/ct5010406.
(37) Feller, S. E.; Zhang, Y.; Pastor, R. W.; Brooks, B. R. Constant Pressure Molecular Dynamics Simulation: The Langevin Piston Method. *J. Chem. Phys.* **1995**, *103* (11), 4613–4621. https://doi.org/10.1063/1.470648.
(38) Essmann, U.; Perera, L.; Berkowitz, M. L.; Darden, T.; Lee, H.; Pedersen, L. G. A Smooth Particle Mesh Ewald Method. *J. Chem. Phys.* **1995**, *103* (19), 8577–8593. https://doi.org/10.1063/1.470117.
(39) Miyamoto, S.; Kollman, P. A. Settle: An Analytical Version of the SHAKE and RATTLE Algorithm for Rigid Water Models. *J. Comput. Chem.* **1992**, *13* (8), 952–962. https://doi.org/10.1002/jcc.540130805.
(40) Phillips, J. C.; Braun, R.; Wang, W.; Gumbart, J.; Tajkhorshid, E.; Villa, E.; Chipot, C.; Skeel, R. D.; Kalé, L.; Schulten, K. Scalable Molecular Dynamics with NAMD. *J. Comput. Chem.* **2005**, *26* (16), 1781–1802. https://doi.org/10.1002/jcc.20289.
(41) MacKerell, A. D.; Bashford, D.; Bellott, M.; Dunbrack, R. L.; Evanseck, J. D.; Field, M. J.; Fischer, S.; Gao, J.; Guo, H.; Ha, S.; Joseph-McCarthy, D.; Kuchnir, L.; Kuczera, K.; Lau, F. T.; Mattos, C.; Michnick, S.; Ngo, T.; Nguyen, D. T.; Prodhom, B.; Reiher, W. E.; Roux, B.; Schlenkrich, M.; Smith, J. C.; Stote, R.; Straub, J.; Watanabe, M.; Wiórkiewicz-Kuczera, J.; Yin, D.; Karplus, M. All-Atom Empirical Potential for Molecular Modeling and Dynamics Studies of Proteins. *J. Phys. Chem. B* **1998**, *102* (18), 3586–3616. https://doi.org/10.1021/jp973084f.
(42) Humphrey, W.; Dalke, A.; Schulten, K. VMD: Visual Molecular Dynamics. *J. Mol. Graph.* **1996**, *14* (1), 33–38. https://doi.org/10.1016/0263-7855(96)00018-5.

(43) UniProt Consortium. The Universal Protein Resource (UniProt). *Nucleic Acids Res.* **2008**, *36* (Database issue), D190-195. https://doi.org/10.1093/nar/gkm895.
(44) Katoh, K.; Standley, D. M. MAFFT Multiple Sequence Alignment Software Version 7: Improvements in Performance and Usability. *Mol. Biol. Evol.* **2013**, *30* (4), 772–780. https://doi.org/10.1093/molbev/mst010.
(45) Waterhouse, A. M.; Procter, J. B.; Martin, D. M. A.; Clamp, M.; Barton, G. J. Jalview Version 2--a Multiple Sequence Alignment Editor and Analysis Workbench. *Bioinforma. Oxf. Engl.* **2009**, *25* (9), 1189–1191. https://doi.org/10.1093/bioinformatics/btp033.
(46) Sheldon, A. L.; González, M. I.; Robinson, M. B. A Carboxyl-Terminal Determinant of the Neuronal Glutamate Transporter, EAAC1, Is Required for Platelet-Derived Growth Factor-Dependent Trafficking. *J. Biol. Chem.* **2006**, *281* (8), 4876–4886. https://doi.org/10.1074/jbc.M504983200.
(47) Fenollar-Ferrer, C.; Stockner, T.; Schwarz, T. C.; Pal, A.; Gotovina, J.; Hofmaier, T.; Jayaraman, K.; Adhikary, S.; Kudlacek, O.; Mehdipour, A. R.; Tavoulari, S.; Rudnick, G.; Singh, S. K.; Konrat, R.; Sitte, H. H.; Forrest, L. R. Structure and Regulatory Interactions of the Cytoplasmic Terminal Domains of Serotonin Transporter. *Biochemistry* **2014**, *53* (33), 5444–5460. https://doi.org/10.1021/bi500637f.
(48) Khelashvili, G.; Doktorova, M.; Sahai, M. A.; Johner, N.; Shi, L.; Weinstein, H. Computational Modeling of the N-Terminus of the Human Dopamine Transporter and Its Interaction with PIP2-Containing Membranes. *Proteins* **2015**, *83* (5), 952–969. https://doi.org/10.1002/prot.24792.
(49) Khelashvili, G.; Stanley, N.; Sahai, M. A.; Medina, J.; LeVine, M. V.; Shi, L.; De Fabritiis, G.; Weinstein, H. Spontaneous Inward Opening of the Dopamine Transporter Is Triggered by PIP2-Regulated Dynamics of the N-Terminus. *ACS Chem. Neurosci.* **2015**, *6* (11), 1825–1837. https://doi.org/10.1021/acschemneuro.5b00179.
(50) Cheng, M. H.; Bahar, I. Molecular Mechanism of Dopamine Transport by Human Dopamine Transporter. *Struct. Lond. Engl. 1993* **2015**, *23* (11), 2171–2181. https://doi.org/10.1016/j.str.2015.09.001.
(51) Yuan, Y.; Huang, X.; Zhu, J.; Zhan, C.-G. Computational Modeling of Human Dopamine Transporter Structures, Mechanism and Its Interaction with HIV-1 Transactivator of Transcription. *Future Med. Chem.* **2016**, *8* (17), 2077–2089. https://doi.org/10.4155/fmc-2016-0138.
(52) Castellana, M. C.; Castellar Montes, A.; Sprague, J. E.; Mahfouz, T. M. A High-Quality Homology Model for the Human Dopamine Transporter Validated for Drug Design Purposes. *Chem. Biol. Drug Des.* **2019**, *93* (5), 700–711. https://doi.org/10.1111/cbdd.13495.
(53) Vergara-Jaque, A.; Fong, P.; Comer, J. Iodide Binding in Sodium-Coupled Cotransporters. *J. Chem. Inf. Model.* **2017**, *57* (12), 3043–3055. https://doi.org/10.1021/acs.jcim.7b00521.
(54) Vergara-Jaque, A.; Palma-Cerda, F.; Lowet, A. S.; de la Cruz Landrau, A.; Poblete, H.; Sukharev, A.; Comer, J.; Holmgren, M. A Structural Model of the Inactivation Gate of Voltage-Activated Potassium Channels. *Biophys. J.* **2019**, *117* (2), 377–387. https://doi.org/10.1016/j.bpj.2019.06.008.
(55) Lodowski, D. T.; Pitcher, J. A.; Capel, W. D.; Lefkowitz, R. J.; Tesmer, J. J. G. Keeping G Proteins at Bay: A Complex between G Protein-Coupled Receptor Kinase 2 and Gbetagamma. *Science* **2003**, *300* (5623), 1256–1262. https://doi.org/10.1126/science.1082348.

(56) Gulati, S.; Jin, H.; Masuho, I.; Orban, T.; Cai, Y.; Pardon, E.; Martemyanov, K. A.; Kiser, P. D.; Stewart, P. L.; Ford, C. P.; Steyaert, J.; Palczewski, K. Targeting G Protein-Coupled Receptor Signaling at the G Protein Level with a Selective Nanobody Inhibitor. *Nat. Commun.* **2018**, *9* (1), 1–15. https://doi.org/10.1038/s41467-018-04432-0.

(57) Torres, G. E.; Amara, S. G. Glutamate and Monoamine Transporters: New Visions of Form and Function. *Curr. Opin. Neurobiol.* **2007**, *17* (3), 304–312. https://doi.org/10.1016/j.conb.2007.05.002.

(58) Khoury, G. A.; Smadbeck, J.; Kieslich, C. A.; Floudas, C. A. Protein Folding and de Novo Protein Design for Biotechnological Applications. *Trends Biotechnol.* **2014**, *32* (2), 99–109. https://doi.org/10.1016/j.tibtech.2013.10.008.

(59) Tsai, C.-J.; Marino, J.; Adaixo, R.; Pamula, F.; Muehle, J.; Maeda, S.; Flock, T.; Taylor, N. M.; Mohammed, I.; Matile, H.; Dawson, R. J.; Deupi, X.; Stahlberg, H.; Schertler, G. Cryo-EM Structure of the Rhodopsin-Gαi-Bγ Complex Reveals Binding of the Rhodopsin C-Terminal Tail to the Gβ Subunit. *eLife 8*. https://doi.org/10.7554/eLife.46041.

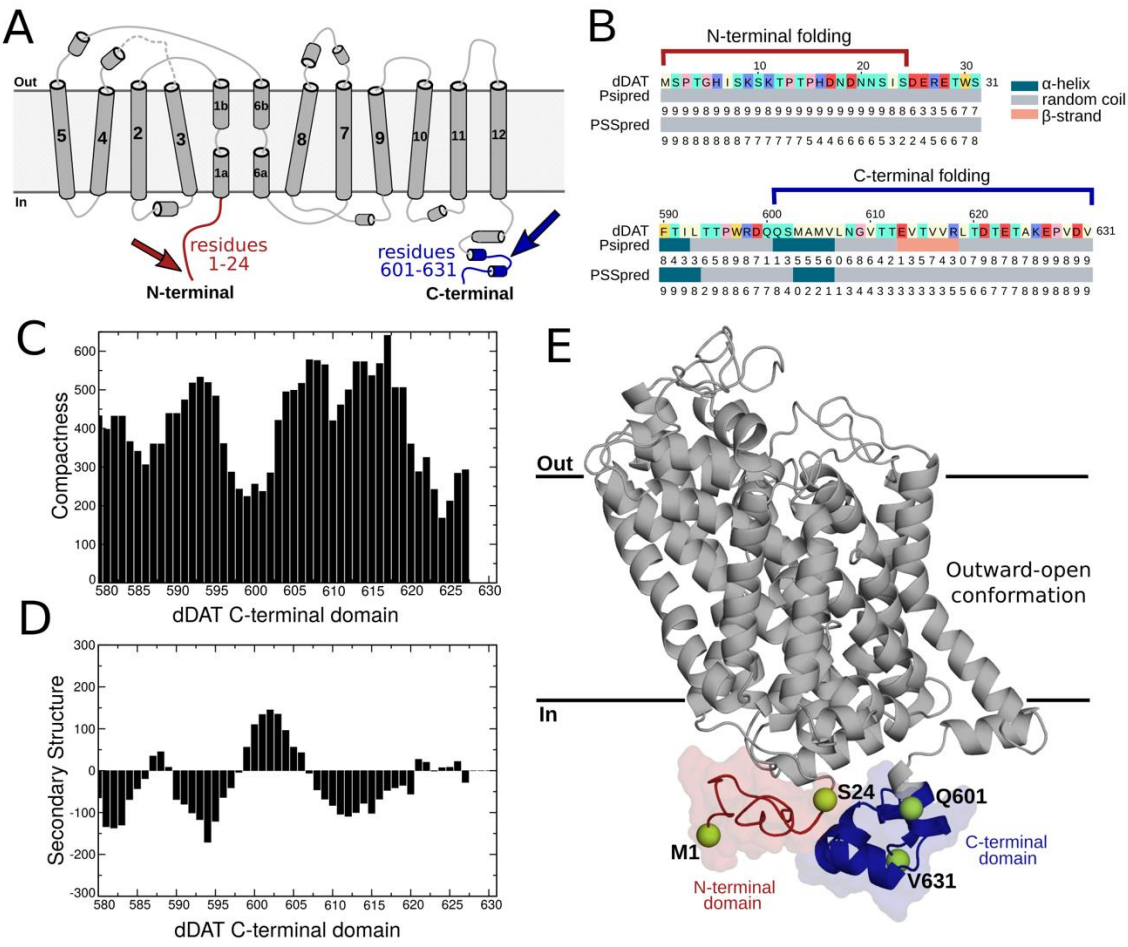

Figure 1: Structural modeling of the N- and C-terminal domains of dDAT. (A) Schematic representation of the dDAT topology with the missing N- and C-terminal domains highlighted in red and blue, respectively. (B) Secondary structure prediction of the N- and C-terminal missing residues calculated with PsiPred and PSSpred. The confidence of the predictions is represented on a scale from 0 to 9. The dDAT sequence is colored according to the chemical properties of the residues. (C) Compactness (spatial neighborhood of individual residues) and (D) secondary structure predictions for the dDAT C-terminal domain estimated with the meta-structure-based approach. The data are shown as a function of residue positions. Large compactness values indicate residues buried in the interior of the 3D structure. Positive secondary structure prediction values are indicative of α-helical segments. (E) Cartoon representation of the selected full-length dDAT model with the N- and C-terminal domains colored according to the topology. The Cα atoms of the initial and final residues modeled in each case are highlighted as yellow spheres.

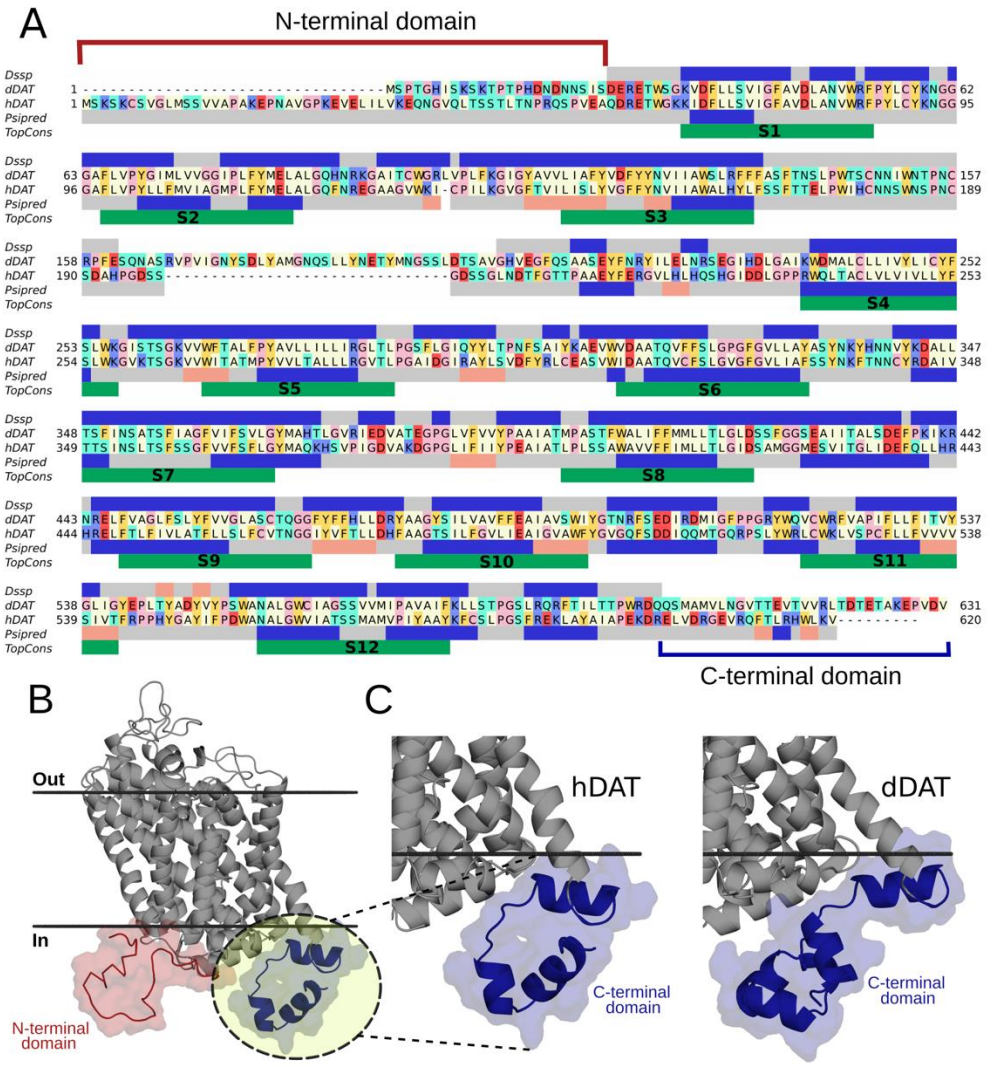

Figure 2: Comparative model of hDAT based on dDAT. (A) Sequence alignment used for hDAT modeling, colored according to the chemical properties of the residues: light yellow, aliphatic (A, I, L, M, and V); cyan, polar uncharged (N, Q, S, and T); yellow, aromatic (F, W, and Y); red, acidic (D and E); light blue, basic (K, R, and H); pink, exceptional (C, G and P). The secondary structure assignment for the dDAT crystal structure (mostly helices in blue bars) was obtained with DSSP, whereas predictions of secondary structure and transmembrane segments (green bars) for hDAT were calculated with PsiPred and TOPCONS, respectively. The N- and C-terminal domains refined with ROSETTA are indicated in the alignment. (B) Cartoon representation of the hDAT model with the C-terminal domain highlighted in a yellow circle. (C) Structural comparison of the C-terminal domain in dDAT and hDAT.

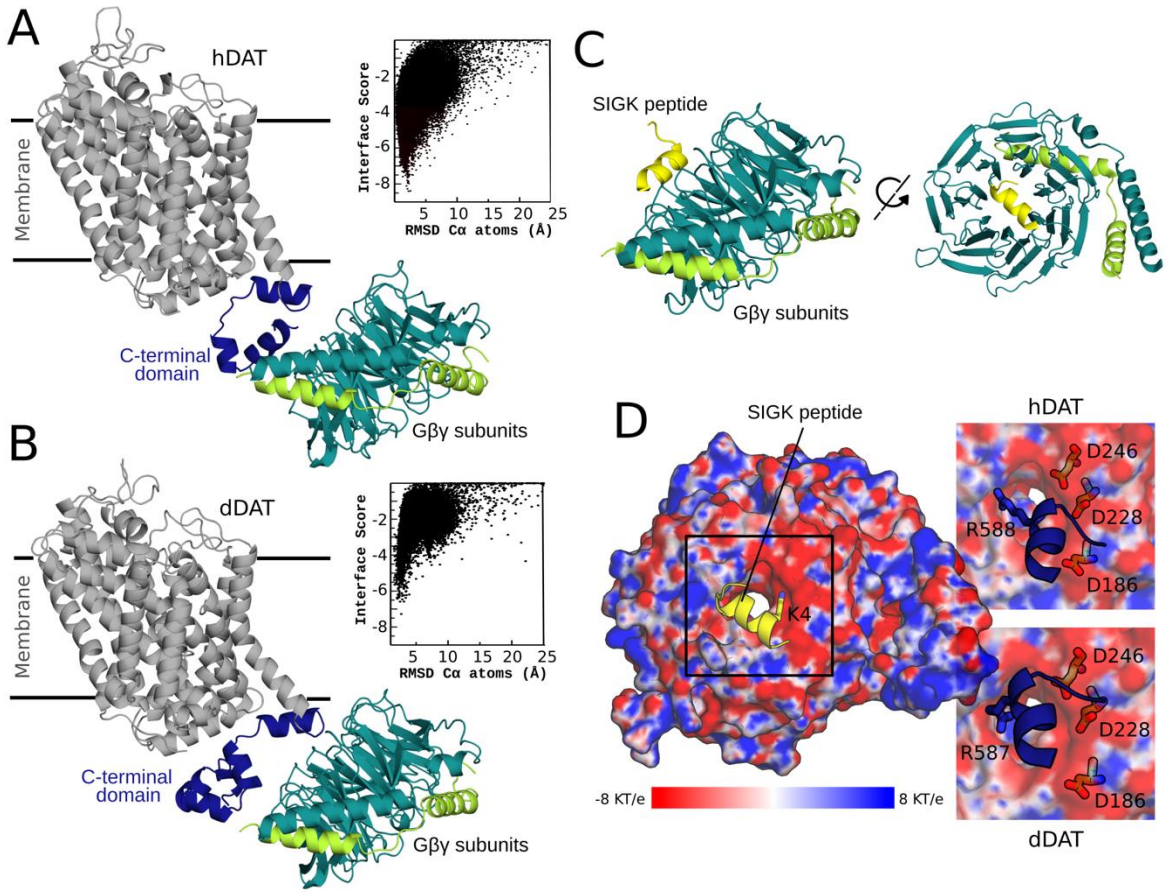

Figure 3: Association of hDAT and dDAT with Gβγ Subunits. Cartoon representation of the lowest-scoring docking conformation of (A) hDAT and (B) dDAT (in gray) in complex with the G-protein βγ subunits (in cyan and green, respectively). The C-terminal region of the transporters selected as the contact area for docking is shown in blue. The insets show the ROSETTA interface score plotted against the Cα RMSD of the docking conformations relative to starting conformation used for docking. (C) Binding surface of the SIGK peptide (in yellow) in the Gβγ crystal structure. (D) Electrostatic surface potential of the Gβ subunit exhibiting an electronegative region (in red) that binds the K4 residue of the SIGK peptide (in yellow). Residues R588 of hDAT and R587 of dDAT interact with the same pocket comprising residues D186, D228 and D246 in the Gβ subunit.

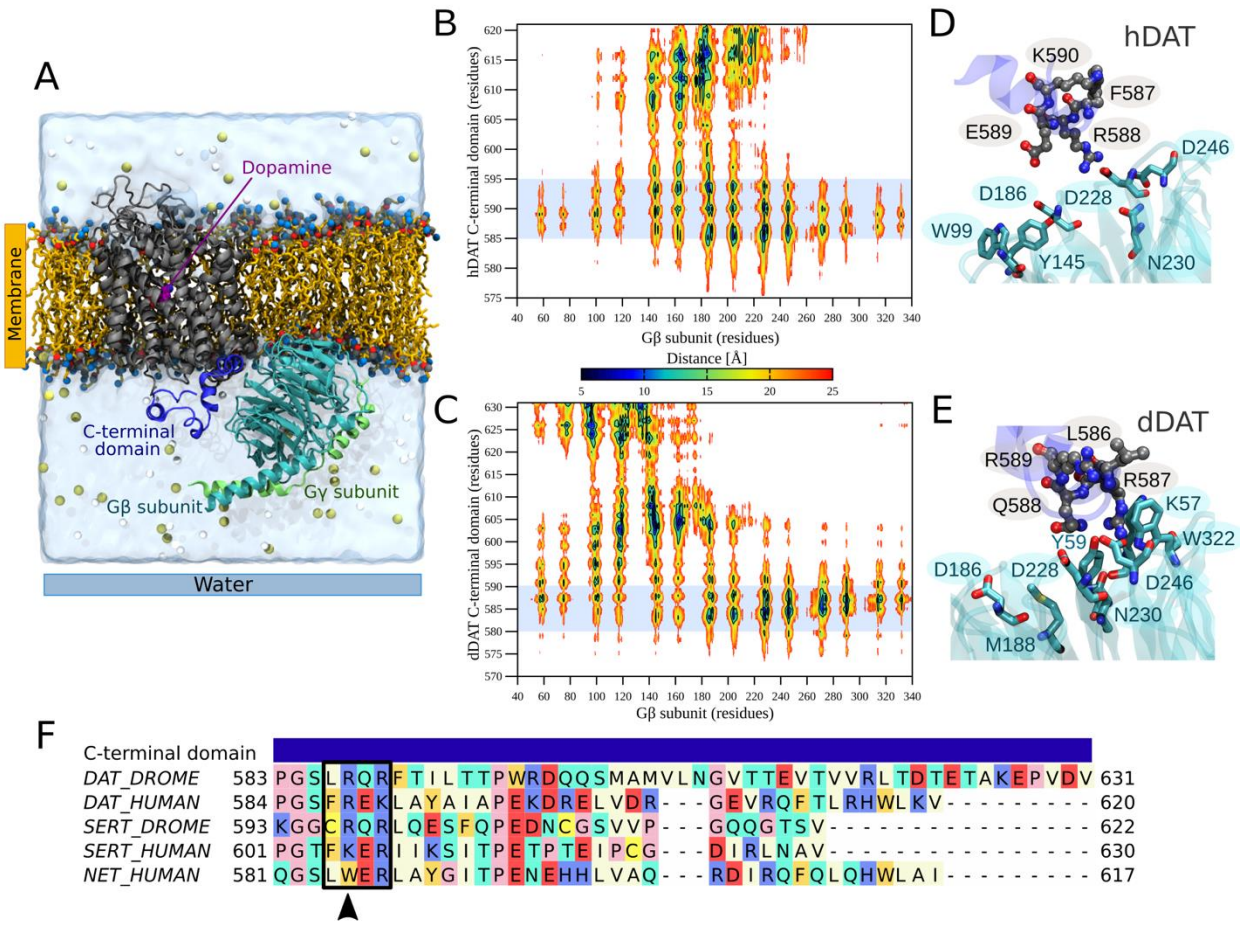

Figure 4: Key residues in the binding interface of hDAT/dDAT and Gβγ subunits. (A) Representative all-atom simulation system for the DAT:Gβγ complexes. DAT, the C-terminal domain, and the Gβ and Gγ subunits are shown by gray, blue, cyan and green cartoon representations, respectively. POPC lipids are displayed in yellow sticks with the head group atoms represented as spheres. TIP3P water molecules are illustrated by a blue transparent surface. Na^+ and Cl^- ions are shown in dark yellow and white spheres, while the dopamine molecule bound to DAT is shown in purple spheres. (B) Contact map showing the average distance between the center of mass of the residue's side chains of hDAT and (C) dDAT and the G-protein β subunit. X and Y axes indicate the position of the residues for each protein. The color scale of the distances ranges from 5 to 25 Å, with larger distances indicated by white. (D) Residues predicted to coordinate the hDAT:Gβγ and (E) dDAT:Gβγ complexes. The residues are displayed as sticks colored by atom type − carbon in gray (hDAT and dDAT) or cyan (Gβ subunit), oxygen in red, nitrogen in blue, and sulfur in yellow. (F) Multiple sequence alignment between DAT, SERT and NET (of *Drosophila melanogaster* (DROME) and human) showing the conservation of the residues identified to bind Gβγ subunits to dDAT and hDAT (black rectangle). The alignment shows only the C-terminal domain sequences of the transporters colored according to the chemical properties of the residues.